Experimental Studies of Gas Permeation through Microporous Silica Membranes

Tomohisa Yoshioka, Eisuke Nakanishi, Toshinori Tsuru, and Masashi Asaeda
Dept. of Chemical Engineering, Hiroshima University, Higashi-Hiroshima, 739-8527 Japan

Permeation mechanism of inorganic gases was studied experimentally and theoretically through microporous silica membranes prepared by the sol−gel method. Inorganic gas permeation was measured using the membranes with subnano pores in diameter. The permeance of He increased with increasing temperature for various cases, while that of CO_2, O_2 and N_2 decreased. In particular, the observed temperature dependency of CO_2 was greater than those of other gases. In such small pores, the interaction energy between a permeant molecule and the pore wall can affect gas-permeation properties. A simple gas-permeation model is used considering the effect of the attractive or repulsive pore-wall potential field, which deviates from the ambient gas phase of the gas molecule concentration (pressure) in a pore. The model can explain the experimental gas-permeation properties successfully. Potential curves of CO_2 and N_2 in a silica pore were also calculated to predict the permeation ratio of CO_2/N_2. This model can help understand further the gas-permeation mechanism in micropores.

Introduction

In recent years, the development of many types of inorganic porous membranes, including sol−gel-derived ceramic membranes, CVD modified membranes, and zeolite membranes, has been reported (Lange et al., 1995). Such membranes have very small pores (micropores), which are less than 1 nm in diameter. Gas-separation processes using microporous inorganic membranes appear to be a very promising technology. Since porous inorganic membranes have relatively good chemical and thermal resistance, they would be expected to be useful under severe conditions where organic membranes cannot be readily applied. The mechanisms of gas permeation and separation for inorganic microporous membranes are different from those for organic membranes. It is generally recognized that gas transport mechanisms through polymeric membranes are controlled by the solution and diffusion processes of the permeating gases. On the contrary, for inorganic porous membranes that have rigid and stable porous structures, the gases permeate through the narrow but permanent open pore space. Sufficient information on gas-permeation properties in porous inorganic membranes, with respect to obtaining general conclusions on permeation mechanisms is not currently available. This is one of the reasons for the absence of commercial evaluations of such membranes for gas separation. Therefore, a quantitative understanding of gas permeation in such porous membranes is important for the development of porous inorganic membranes, which can be efficiently applied to new gas-separation processes, for example, the separation of CO_2/N_2.

The transport mechanism of gases through microporous membranes is usually classified as Knudsen diffusion and surface diffusion (Li and Hwang, 1991). Hwang and Kammermeyer have derived a gas transport equation that considers the total flow rate of gases as the sum of the gas-phase flow and the surface flow (Hwang and Kammermeyer, 1966), given by Eq. 1

$$Q\sqrt{MT} = A + BT\exp(\Delta/T), \tag{1}$$

where Q is the gas permeability, and A is a geometrical constant for gas-phase flow; that is, the first term of the right-hand side indicates the Knudsen flow. The symbol Δ is related to the difference between the adsorption energy and the activation energy. This model was evaluated by applying it to data on the permeation of several gases by a Vycor mi-

Correspondence concerning this article should be addressed to T. Yoshioka.

croporous glass membrane (mean pore diameter is 4 nm), and was modified to express pressure dependency of permeabilities using the Freundlich adsorption isotherm (Li and Hwang, 1991, 1992). These models are capable of yielding the minimum of the modified permeability $Q(MT)^{0.5}$ when it is plotted against temperature, which was experimentally observed for the permeation of several gases through Vycor glass membranes.

Nicholson and Petropoulos (1973) considered the influence of the pore-wall potential on the permeating gaseous molecules at the pore center. They studied the effect of pore size, pore shape (slit and cylinder), and the strength of gas–surface interaction on the permeation flux of gases and explained qualitatively the results reported by Hwang and Kammermeyer (1966).

Shindo et al. (1983) also adopted a parallel-flow model to explain the gas-permeation properties through porous Vycor glass membranes. They evaluated the partition coefficient between the surface phase and the "gas phase" in a pore by considering the potential energy between a gas molecule and the solid surface, and derived an equation that described the surface flow flux. As for the gas-phase flow, they assumed that the molecules passed through the force field by the solid surface, which would serve to bend the trajectories of the gas-phase molecules. They concluded that the gas-phase flow rate therefore became smaller than the ideal gas-flow rate. It is very interesting that their model equation was derived without the assumption of any physical adsorption model. This model also satisfactorily explained some experimental data as well as the model by Hwang et al. (1991, 1992).

Those models just described, which were studied using Vycor glass membranes, are for gas permeation through a pore whose diameter is larger than 1 nm. It would be unsuitable, however, to apply them to gas permeation phenomena in subnano order pores, since the distinction between the gas phase and the surface phase in such pores may be very difficult or meaningless.

On the other hand, gas-permeation theory in micro- or subnano pores has been studied for zeolite or modified glass membranes. Gas diffusion mechanisms in such very small pores can be explained as an activated process based on the configurational diffusion (micropore diffusion) theorem, which is described by the Eyring equation as Eq. 2 (Xiao and Wei, 1992a)

$$D = D^{+} \exp\left(-\frac{E}{RT}\right). \tag{2}$$

In those pores, the apparent activation energy E is larger than zero. Xiao and Wei assumed that the value of E was equal to the difference between the potential in two different types of pores in zeolite, a channel pore and an intersection one. They calculated the value for E for several gas species from the zeolitic pore structure by using Lennard-Jones potential as the gas–framework interaction function. As a result, they concluded that the transition from Knudsen diffusion to a configurational one was dependent on the properties of the diffusing molecules and those of zeolites (pore structure) (Xiao and Wei, 1992a). Their diffusion-model equation contains no unknown parameters, and therefore, the activation energy and the diffusion coefficient can be evaluated if the pore structure and the physical properties of the diffusing gas molecules (LJ parameters) are given. They studied diffusivities of hydrocarbons in zeolites theoretically and performed experimental analysis through adsorption and diffusion experiments using zeolite powder (Xiao and Wei, 1992b).

The permeation mechanisms through membranes that have subnano pores were discussed by the authors described below. Lange et al. (1995) considered that the apparent activation energy of permeation through membranes could be described as the difference between the isosteric heat of adsorption and the genuine activation energy for micropore diffusion. In their study, the isosteric heat was calculated from some adsorption isotherms under different temperatures for nonsupported membranes by using the Clasius-Clapeyron equation. They evaluated the genuine activation energy for the diffusion of several gases through a sol–gel-derived ceramic membrane, which has smaller pores than zeolite 4A.

Shelekhin et al. (1995) have proposed that the activated permeation behaviors of nitrogen or carbon dioxide gases for glass membranes can be treated as the summation of the activated diffusion in the gas phase and in the adsorption phase. They used the Dubinin-Radushkevich adsorption model and successfully explained not only the experimental temperature dependency of the permeabilities but also the pressure dependency. This may be because they considered the transport of the adsorption phase in terms of activated diffusion. However, based on the micropore filling theorem, the gaseous activated diffusion mechanism within the adsorption phase is still not clear.

The models of both Lange and Shelekhin describe the gas-permeation mechanism through a micropore that considers the effect of the pore-wall potential (adsorption energy). These models can explain not only the activated permeation process where the permeation flux increases with increasing temperature but also predict or explain the "surface diffusion-like temperature dependency," where the permeance decreases with increasing temperature. Temperature dependence of permeance is decided by the relative magnitude of two counteracting contributions of a kinetic one (diffusion) and an equilibrium one (adsorption). The negative temperature dependence of permeance, which can be seen in the case of permeation of CO_2 and hydrocarbon gases in the temperature range from room temperature to about 300°C. This temperature dependency might be caused by the dominant contribution of the pore-wall "attractive" potential. This phenomenon has been recognized as the surface diffusion process for permeation through relatively larger pores, that is, nanoscale pores. The objectives of this study are to fabricate molecular sieving microporous silica membranes that have narrow enough pore-size distributions to be effective for CO_2/N_2 gas separation, and to analyze pore size and gas species dependence of the permeation property through such small pores by using a simple gaseous permeation model. In this work, some microporous silica membranes were prepared by a sol–gel method, and the mean pore size was controlled, so as to be slightly different from each other. The temperature dependencies of permeation fluxes of several gases were then measured for each membrane. Since the strength of the interaction between the permeant gas molecules and the pore surface is dependent on pore size, we

were able to study gaseous permeation mechanisms within different micropore size, from the standpoint of the attractive or repulsive potential field in the micropores. The model calculations for predicting the permeance and the permeation ratio for CO_2/N_2 system were also performed based on the gas-permeation model.

Experimental Studies

Membrane preparation

The microporous silica membranes used in this study were prepared by the sol–gel method, which is comprised of two steps: (1) preparation of the colloidal sols, and (2) sol-coating on porous substrate and firing (Asaeda et al., 1993). The silica colloidal-sol solutions were prepared through hydrolysis (for 1 h at room temperature), polymerization, and condensation (for about 12 h at the boiling point) of $Si(OC_2H_5)_4$ aqueous solutions with a small amount of acid (HNO_3) as the catalyst. Silanol compounds that have some −OH groups would be generated at the hydrolysis stage and they would be combined linearly or three dimensionally in long silica polymers at the polymerization and condensation stage. Complicated interweaving of these polymers would lead to the first SiO_2 particles composed of siloxane bonds, and these first particles could cluster to be larger second particles through aging. The mean particle diameter of the colloidal sol could be controlled by changing the concentration of $Si(OC_2H_5)_4$ in water in the starting solution. In this work, four types of colloidal silica sol were prepared from their polymer solutions of different concentrations, which are listed in Table 1. These colloidal-sol solutions, whose mean colloidal-sol particle diameters were different from each other, ranging from several nanometers to some tens of nanometers, were coated on cylindrical porous α-alumina supports (OD: 10 mm; length: 90 mm), which had been heated at 180–190°C before coating. The coating was done by making a cloth that had been wet with the colloidal sols, gently contacting the hot substrate. These hot-coating procedures allow gelation to occur instantly on the substrate and prevents the sol from penetrating deep into the substrate pores, which results in the formation of a very thin separation layer. After colloid coating, the membrane was fired at 360–570°C for about 15 min in air. After repeating the coating and firing procedures several times with each colloidal sol in the order of its particle size, subnano pore membranes were obtained. We fabricated four membranes of different pore size (Membranes A, B, C, and C′) for gas-permeation experiments by choosing the colloidal size at the final coating. Membrane C′ was obtained from the modification of Mem.-C by water-vapor treatment; after the water-vapor permeation treatment on Mem-C, the membrane was dried at 300°C.

Table 1. Preparation of Colloidal Silica Sols

	$Si(OC_2H_5)_4$ [wt. %]	HNO_3 [g]	Total H_2O [g]	Mean Particle Size* [nm]
Sol-1	2.0			≈ 80
Sol-2	1.5			40–60
		2.0	500	
Sol-3	1.0			20–40
Sol-4	0.5			< 20

*Measured by dynamic light scattering method (ELS-800, OTUKA ELECTRONICS CO., LTD.).

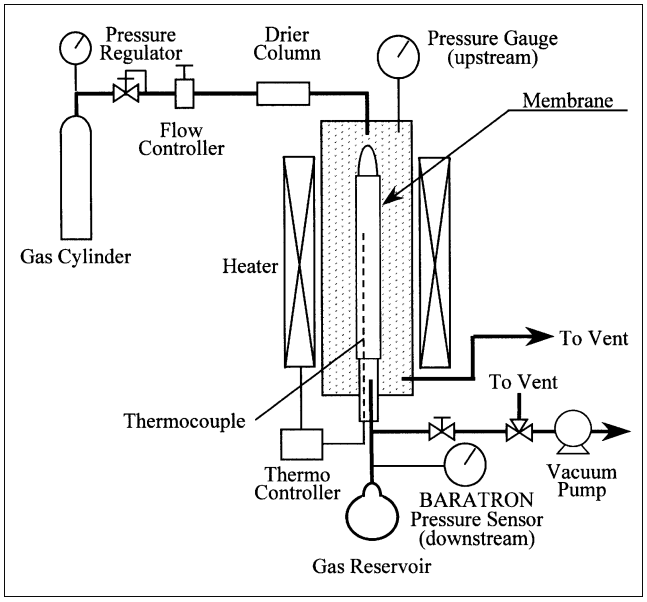

Figure 1. Experimental apparatus for permeance measurements.

Permeation and adsorption

Figure 1 shows the experimental apparatus used for the permeance measurements with inorganic gases, H_2, He, CO_2, O_2, N_2, Ar, and some organic gases, CH_4, C_2H_4, C_3H_8, among others. A cylindrical membrane module was mounted in a temperature controlled cell, as shown in the figure. The upstream pressure was controlled at 0.1 MPa by a pressure regulator and mass flow-controller, while the downstream portion of the membrane was evacuated by a vacuum pump. That is, the pressure difference across the membrane was about 0.1 MPa. The flow rate of the permeant was calculated from the volume of the gas reservoir and the rate of pressure increase after the downstream line to the vacuum pump was closed (quasi-steady-state flow method). Gas permeation experiments were performed in a temperature range from 30°C to 300°C. Membranes prepared by using the same colloidal sols showed almost the same gas permeation properties. That is, the reproducibility of such sol–gel membranes was sufficiently good. In addition, in dry gas-permeation experiments, these silica membranes showed stable gas permeability for several weeks, while under the water-vapor coexistence condition, the decrease of the permeation flux along with time could be observed. Therefore, as shown in Figure 1, the gases used in permeance measurements were supplied to the membrane module after passing through a dryer column filled with molecular sieve 3A, dehumidification agent, in order to remove the small amount of moisture in the gases, especially in CO_2 and the organic ones.

In order to examine the strength of the interaction between the silica surface and the permeating gas molecules,

adsorption experiments on nonsupported silica powder were performed using volumetric adsorption equipment for CO_2 and N_2 gases. The adsorbent (silica powder) was obtained by drying and firing the silica colloidal-sol solution that was used to prepare silica membranes.

Results and Discussion

Conventional transport models

Conventional gas-permeation or-diffusion mechanisms through a pore have been reviewed by a number of authors (Xiao and Wei, 1992a; Shelekhin et al., 1995; Burggraaf, 1999).

The gas-molecule permeation mechanism on microporous membranes is largely dependent on their pore size. When the pore diameter ranges from 1 nm to several nm, that is, the pore diameter is approximately equal to the mean free path of a molecule, the passage of gas molecules through a pore obeys the Knudsen diffusion theory. According to Fick's first law of diffusion, the diffusive flux in a given direction is related to the gradient of the concentration by a phenomenological relation, Eq. 3

$$J = -D\frac{dc}{dx}, \tag{3}$$

where D is the diffusion coefficient, which can be expressed as Eq. 4 for Knudsen diffusion

$$D = \bar{C}\bar{v}\lambda, \tag{4}$$

where parameter C is governed by geometrical factors, $\bar{v}$ is the mean molecular velocity, and λ is the mean free path. Substituting Eq. 4 into Eq. 3, and considering that λ is proportional to the pore diameter d with the relation of Eqs. 5 and 6, Eq. 7 is obtained

$$\bar{v} = \left(\frac{8RT}{\pi M}\right)^{0.5} \tag{5}$$

$$c = \frac{p}{RT} \quad \text{(ideal gas relation)} \tag{6}$$

$$J = -Cd\left(\frac{8RT}{\pi M}\right)^{0.5}\frac{dc}{dx} = Cd\left(\frac{8}{\pi MRT}\right)^{0.5}\frac{\Delta p_a}{L}, \tag{7}$$

where Δp_a is the pressure drop as the driving force for diffusion across the diffusion length L. Consequently, the classic Knudsen permeation coefficient P_K is described as Eq. 8 with the parameter C_K, which is only dependent on the pore geometry

$$P_K = \frac{J}{\Delta p_a} = \frac{C_K}{\sqrt{MRT}}. \tag{8}$$

Since permeance is inversely proportional to the square root of the molar weight, in the case of the separation of CO_2/N_2, for example, the permeation ratio expected from the Knudsen mechanism is only 0.8. This degree of permeability difference is not sufficient for application to actual separation processes.

For microporous membranes that have a pore size nearly equal to the diameter of permeating molecules, a molecular sieving like separation, the origin of which is the differences in molecular shape and size, might be expected. The number of molecules with kinetic energy larger than the activation energy for permeation is proportional to $\exp(-E_A/RT)$, assuming a Maxwellian velocity distribution of molecules. The permeation coefficient P_A for the activated diffusion mechanism can be expressed as Eq. 9

$$P_A = C_A \exp\left(-\frac{E_A}{RT}\right), \tag{9}$$

where C_A is a constant depending on the system, E_A is the apparent activation energy described as the difference between the adsorption energy and a substantial activation one for diffusion in a micropore. When the permeation flux by the activated diffusion is dominant, the permeability has a tendency to increase along with the temperature. Ideally, this mechanism enables gas molecules to separate, while the separation of those gas molecules is difficult if their diameter sizes are similar as in the CO_2(3.3 Å)/N_2(3.64 Å) system. This is because an accurate pore-size control is needed at the subnanometer scale. Moreover, the flux of the permeanting molecule tends to be rather small for such pores.

In the intermediate region from the Knudsen diffusion to the activated diffusion, molecules in a pore are in general thought to move both by Knudsen diffusion in the gas phase and by surface diffusion in the adsorbed phase. According to the surface-diffusion theorem, the high flux of the permeant and the large temperature dependencies of the permeability of adsorbable gas molecules, which cannot be understood by the Knudsen mechanism, can be explained quantitatively. However, the issue of whether the adsorbed phase and the gas phase can be defined even within such the limited space in pores as small as 1 nm or less than 1 nm in diameter is not clear. In addition, the liquid-like adsorption phase of inorganic molecules might be barely formed at room temperature or higher temperature. This is because the critical temperatures of many inorganic gases are generally lower than room temperature, for example, 126 K for N_2, 154 K for O_2, and 304 K for CO_2. Since the inorganic porous membranes of pores less than 1 nm would be expected to be utilized as gas separation membranes for separating inorganic gas mixtures, a clarification of the permeation mechanism in such pores is necessary.

Permeation model considering the effect of the potential field in a micropore

The mechanism of permeation in pores of subnanometer size is different from the Knudsen mechanism, probably because the interaction between a permeating molecule and the pore-wall surface influences the permeation properties of the gases. Petropoulos et al. considered Henry-type adsorption in a pore and transport based on the Knudsen diffusion mechanism to explain the gas-permeation properties within small pores (Petropoulos and Havredaki, 1986; Petropoulos and

Petrou, 1991). These authors carefully considered the gas transport phenomena in the pore-wall potential field and carried out model calculations using realistic pore structures. Those results were compared with the experimental permeation data for mesoporous materials, where surface diffusion on the pore surface and Knudsen diffusion in gas phase occurred. This concept is useful in understanding the gas-permeation mechanisms that are applicable from the Knudsen diffusion region to the activated one. We assumed gaslike diffusion in a simplified (structureless pore wall) potential field, which can be expressed as a function of pore size, and tried to explain the gas-permeation properties through real molecular sieving porous silica membranes.

The simple gas-permeation model equation based on the Henry-type concentration enhancement and the Knudsen diffusion can be derived as follows. In general, when a potential field Ψ is given as a function of location x, the pressure difference at x, $\Delta p = p(x + \Delta x)$-$p(x)$, is described as the product of gas density $\rho(x)$, acceleration $a(x)$, and Δx, according to the classic Newtonian mechanics

$$\Delta p = -\rho(x)a(x)\Delta x. \tag{10}$$

The acceleration $a(x)$ for a gas, in molar units, is

$$a(x) = \frac{1}{M}\frac{d\Psi}{dx}. \tag{11}$$

Substituting Eq. 11 into Eq. 10, we obtain the following differential equation at the limit of $\Delta x \to 0$

$$\frac{dp}{dx} = -\frac{\rho(x)}{M}\frac{d\Psi}{dx}. \tag{12}$$

By using the relation $\rho(x) = pM/RT$ (for ideal gas), we have

$$\frac{dp}{p} = -\frac{d\Psi}{RT}. \tag{13}$$

Integrating Eq. 13 with the boundary condition, $p \to p_0$ at $\Psi(x) \to 0$, we obtain Eq. 14

$$p = p_0 \exp\left(-\frac{\Psi}{RT}\right). \tag{14}$$

Equation 14 can be more easily derived from the condition of the chemical potential equilibrium defined by Eq. 15

$$RT \ln p_0 = RT \ln p + \Psi. \tag{15}$$

Equation 14 indicates that the pressure in a potential field Ψ is exp $(-\Psi/RT)$ times as great as that in a null-potential bulk phase. This relation is well known as the Boltzmann distribution theorem. For example, it is clear that in the gravity potential field on the earth the atmospheric pressure distribution is a function of the distance from the ground.

In a micropore, where the potential field that originates from the pore wall, acts on the permeate-gas molecules, the true pressure or concentration of gases can be described by Eq. 14. The potential is a function of the location within a pore in nature. A detailed analysis of the potential function in micropores is given by Everett and Powl (1976). For a pore of about 1 nm or larger in diameter, the potential tends to show a double minimum near the pore wall for large wall distances. For smaller wall distances, however, it coalesces to a single minimum, which exists at the center of the pore. This is true for micropores that are subnanometer in size, and the depth of the potential well becomes deeper for a smaller pore. This means that the gas molecules largely permeate along the center axis of the pore. Accordingly, the effective pore-wall potential on the permeant gas molecules can be assumed to be approximately the potential at the center, which depends only on pore size. The following assumptions were introduced to derive a simple gas-permeation model equation for micropores (Yoshioka et al., 1998).

1. Gas molecules permeate through cylindrical and straight micropores.

2. A homogeneous potential field, E_P, exists in the radial and lateral directions, and the potential is null outside of the pore.

3. Thermodynamic equilibrium conditions, between the gas phase and the "inner-pore" phase, are satisfied both at pore entrance (upstream) and at pore exit (downstream).

4. Molecules in the pore are transported by their thermal movements.

From assumptions 2 and 3, and Eq. 14, we see that the pressures in the pore at the pore entrance (upstream side), (p_P^u) and the pore exit (downstream side), (p_P^d) are given by Eq. 16

$$p_P^i = p^i \exp\left(-\frac{E_P}{RT}\right), \tag{16}$$

where i indicates u (upstream) or d (down stream). The apparent pressure drop across the membrane is $\Delta p_a = p^u - p^d$, while the effective pressure difference as the driving force for permeation in a pore will be $\Delta p_P = p_P^u - p_P^d$ (see Figure 2).

$$\Delta p_P = \Delta p_a \exp\left(-\frac{E_P}{RT}\right). \tag{17}$$

From assumption 4, the permeation flux J_P must be inversely proportional to $(MRT)^{0.5}$ and considered analogously to Eq. 7

$$J_P = \frac{Cd}{\sqrt{MRT}}\frac{\Delta p_P}{L}. \tag{18}$$

Thus, the permeability coefficient P_P is given by the well-known form of Eq. 19

$$P_P = \frac{J_P}{\Delta p_a} = \frac{C_P}{\sqrt{MRT}} \exp\left(-\frac{E_P}{RT}\right). \tag{19}$$

This model is connected with the Henry law enhancement of density within a micropore. Therefore, it might be only applicable at a temperature higher than critical temperature,

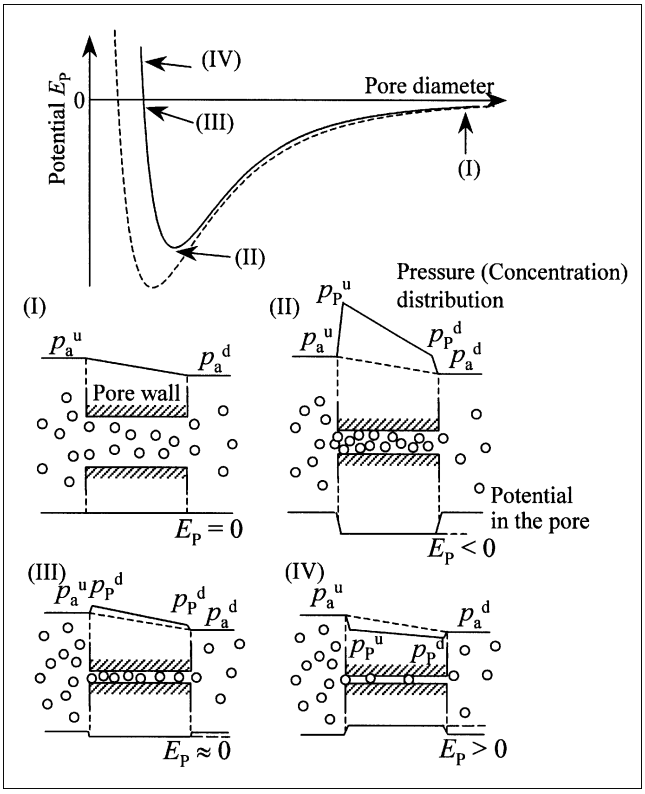

Figure 2. Leveled potential in micropore as a function of pore size (I > II > III > IV) and gas pressure (concentration) distributions in the lateral direction.

where the distinction between the surface adsorption phase and the gas phase in a micropore is insignificant. In such a case, the influence of all guest–guest interactions might be reasonably neglected. On the other hand, this model will fail to explain the permeation properties of gases, at a relatively high pressure and lower temperature region where the liquid-like surface adsorption phase or capillary condensation phase could be formed in a micropore. In nature sol–gel-derived membranes not only have complex and random micropore structures but also a specific sorption site such as silanol groups; however, it would be difficult to validate the realistic pore model quantitatively, as would its applicability. For simplicity, in our model, the transportability, which depends on the irregularities of micropore structures, is involved in the preexponential term, C_P, as a membrane constant, and the potential field, E_P, is given as an averaged one in the direction of permeation. In addition, test gas molecules used in this study have very little specific interaction with the silanol groups, and they have relatively weak van der Waals interaction with the oxygen atoms in siloxane groups (–Si–O–Si–) that cover the majority of the pore surface. Therefore, we assume that, only in this study, the influence of specific sorption sites, such as silanol groups, do not need to be considered in the permeation model. This permeation model might be crude, but would be helpful in understanding the essence of the transport phenomena within such a small space.

As shown in Figure 2, the value of E_P depends on both the pore size and the characteristics of the permeating gas molecule. For relatively large pores (Type I), where E_P is nearly zero, gas molecules permeate by normal Knudsen diffusion. In the case of Type II pores, where E_P is much less than zero, that is, the attractive potential works on permeating molecules, the permeation flux surpasses that by the Knudsen diffusion, because exp $(-E_P/RT)$ is larger than unity, as in the case of surface diffusion. As for Type III, a slightly smaller pore than Type II, the repulsive part of the potential is nearly equal to the attractive one, and E_P is nearly zero. In this case, Eq. 19 results in a formula similar to Eq. 8, and the permeation property is apparently similar to that of the Knudsen mechanism. For much smaller pores (Type IV), where E_P is greater than zero, Eq. 19 can be used to express gas-activated diffusion, which was derived by Shelekhin et al. (1995). When the permeating molecule is a little smaller and has greater interaction with the pore surface, the curve of E_P becomes the broken line, that is, the curve has a deeper bow at the smaller pore diameter than the solid line does.

In the derivation of Eq. 19, which seems to have the same structure as equations reported earlier by Shelekhin et al. (1995) and Lange et al. (1995), only the interaction between a permeating molecule and the pore wall is represented by E_P. This value corresponds to the difference between the adsorption energy, Q_a, and the activation energy for diffusion in a pore, E_d, in their model. If the value of E_d is small enough compared with Q_a to be neglected, E_P is approximately equal to Q_a. By considering the pore size and the permeating-gas molecular properties (size and affinity) dependence of E_P in this model, it can be expected that universal understandings of the permeation mechanisms could be obtained comprehensively in a micropore from Knudsen diffusion to activated diffusion.

Analysis of the experimental observations

Figure 3 shows the observed permeances of gases for Mem.-A and Mem.-B as a function of kinetic diameter (Breck, 1974). Judging from the relation between the permeance and the kinetic diameter of the permeating molecules, both Mem.-A and Mem.-B appear to have pores that are smaller than 5 Å, and Mem.-B has slightly smaller sizes than Mem.-A does. Figures 4a and 4b show the Arrhenius plots of the observed permeance for Mem.-A and Mem.-B, respectively. The permeance of He increased with increasing temperature for both Mem.-A and Mem.-B. These increases represent the activated diffusion. On the other hand, those of CO_2, O_2 and N_2 decreased with increasing temperature. The temperature dependencies of CO_2 permeance for Mem.-A and Mem.-B are very similar to each other, but the slopes of the curves for O_2 and N_2 are larger for Mem.-A than are those for Mem.-B. If a molecule permeates via the Knudsen diffusion mechanism, the dependence of permeance on temperature should be independent of the gas species and pore size; in addition, N_2 can be expected to have a larger permeance than CO_2, since the molar weight of N_2 is smaller than is that of CO_2. The observed results, however, clearly show that their characteristics are contrary to the Knudsen diffusion mechanism. Therefore, the permeation mechanism for both Mem.-A and Mem.-B is different from simple Knudsen diffusion. This was also true for the case of another membrane C and modified

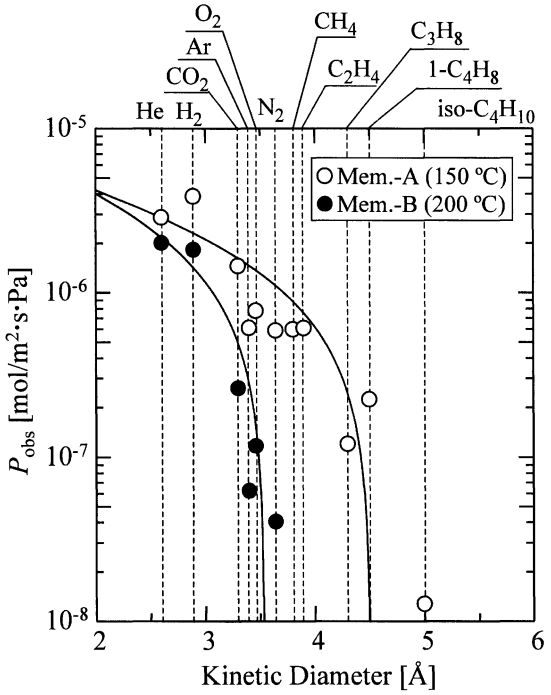

Figure 3. Permeance vs. kinetic diameter for several gas species.

Mem.-C (= Mem.-C′). The observed temperature dependency curves of the permeances of H_2, He, CO_2, and N_2 gases on Mem.-C and -C′ are shown in Figures 5a and 5b, respectively. Judging from these curves, the characteristics of Mem-.C appeared to be almost the same as those of Mem.-B. Membrane C′, however, showed a lower permeance for CO_2 and N_2, and a higher permeation ratio for CO_2/N_2, than did those of Mem.-B or -C (before modification). These changes in membrane characteristics are probably caused by the generation of silanol groups on the pore surface and the subsequent reduction in the effective pore size. Table 2 summarizes the CO_2 permeance and the permeation ratio of

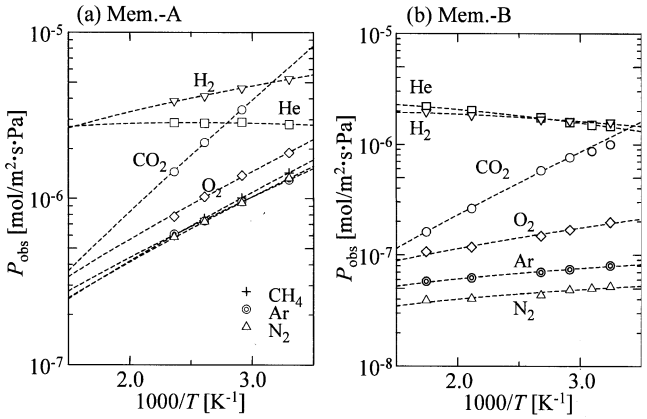

Figure 4. Dependencies of permeance on temperature for membrane A and B (curves fitted with Eq. 19).

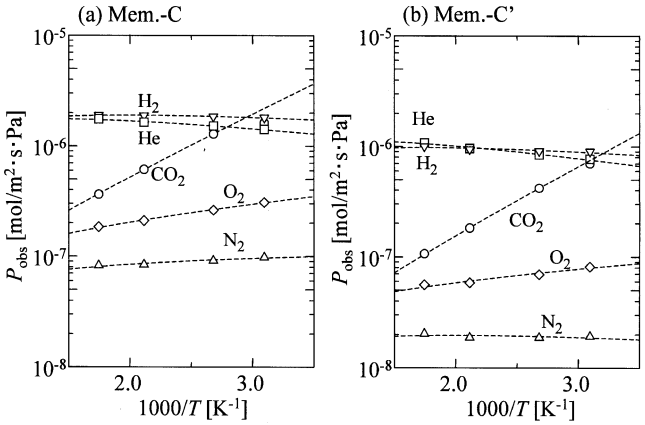

Figure 5. Dependencies of permeance on temperature for membrane C and C′ (curves fitted with Eq. 19).

Table 2. Membranes *A*, *B*, *C*, and *C′* Transport Data for CO_2^*

	300°C		150°		50°C	
	P_{CO_2}	α	P_{CO_2}	α	P_{CO_2}	α
Mem.-A	—	—	1.45×10^{-6}	2.47	—	—
Mem.-B	1.61×10^{-7}	4.12	—	—	8.65×10^{-7}	17.2
Mem.-C	3.62×10^{-7}	4.4	—	—	1.62×10^{-6}	16.6
Mem.-C′	1.07×10^{-7}	5.26	—	—	7.02×10^{-7}	36.5

**Note:* $\alpha = P_{CO_2}/P_{N_2}$, where P_{CO_2} and P_{N_2} indicate the permeance of CO_2 and N_2 in mol/m^2·s·Pa, respectively.

CO_2/N_2 as an index of membrane performance. If molecules move in the pores in accordance with the Knudsen diffusion mechanism or Eq. 8, the values of the experimental permeance, P_{obs}, multiplied by $(MRT)^{0.5}$ should be identical. In Figure 6a, the values of C_K $(= P_{obs}(MRT)^{0.5})$ observed at 150°C are plotted (open circles) against the molar weight for Mem.-A. As can be seen from the figure, these values are not identical, and, in particular, the value for CO_2 has largely deviated from those for the other gases.

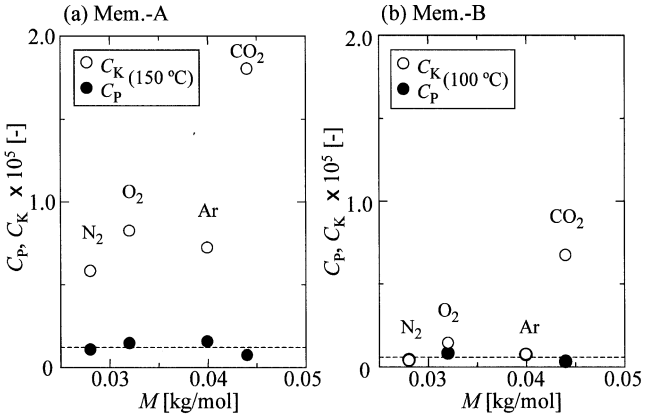

Figure 6. Comparison of C_K $(= P_{obs}(MRT)^{0.5})$ with C_P for several gas species.

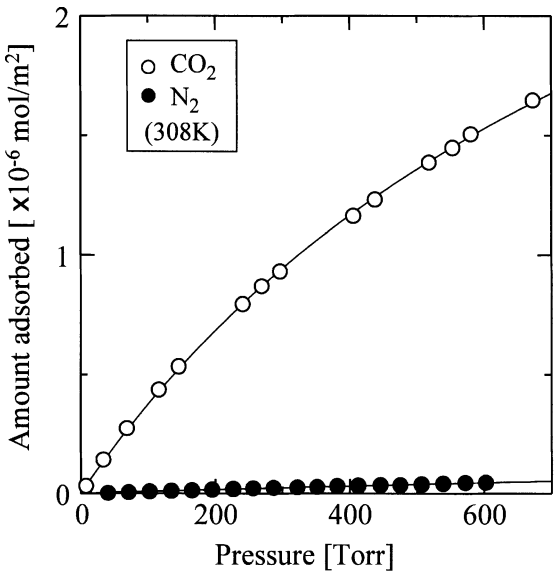

Figure 7. CO_2 and N_2 adsorption isotherms on SiO_2.

Figure 7 shows the observed adsorption isotherms for CO_2 and N_2 on silica powder at 308 K. The molar amount of adsorbed per unit surface area of adsorbent is plotted against the equilibrium gas-phase pressure. A nitrogen-adsorption isotherm at 77 K measured by using BELSORP28SA (Bel Japan, Inc.) shows that the surface area, S_A, is 417 m^2/g-adsorbent as BET surface area (Brunauer et al., 1938). The amount of adsorbed CO_2 is larger than that of N_2 under identical gas pressure. This indicates that the affinity of CO_2 for the silica surface is relatively large compared with that of N_2. Since the temperature dependencies of permeance of CO_2 are also larger than that of N_2 on Mem.-A, -B, -C and -C′, these findings suggest that the interaction between permeating gas molecules and pore surface could play an important role in the permeating the molecules through porous silica membranes.

According to the gas-permeation model mentioned earlier, the permeance can be given by Eq. 19 with parameters C_P and E_P. As shown in Figure 4a, Eq. 19 gives a good fit to the experimental data. The values of C_P and E_P fitted by Eq. 19 are summarized in Table 2. The value of E_P for CO_2 is relatively small (the absolute value is large) compared to those of O_2 and N_2, which are also negative. The fact that the absolute value of E_P of CO_2 is larger than that of N_2 is consistent with the experimental results of adsorption, as shown in Figure 7. These results indicate that the pore-wall potential field attracts CO_2 to increase the permeance and that even O_2 or N_2 are effectively attracted to the pore wall. The values of C_P for several gases are plotted by the solid circles in Figure 6a. In comparison with the observed C_K (open circles) in wide dispersion, the values of C_P are nearly identical for CO_2, Ar, O_2, and N_2. The values of C_P and E_P for Mem.-B are also summarized in Table 2, and the values of C_P are plotted in Figure 6b. The values of C_P are nearly identical, as they are for Mem.-A. However, it should be noted that the values of C_K for Ar, O_2, and N_2 are very close to those of C_P for Mem.-B. This means that the pore-wall potential field had no dramatic effect on these gases; therefore, their permeation mechanisms are apparently simply Knudsen diffusion. Since Mem.-B has smaller pores than Mem.-A, as shown in Figure 3, and the kinetic diameter of CO_2 is smaller than those of the others, only CO_2 could feel an attractive potential in the pores of Mem.-B. If the pore size was much smaller than that of Mem.-B, the value of E_P for those gases might be positive (repulsive potential), and their permeation properties would be activated diffusion.

As for H_2 and He, the permeation characteristics are obviously different from those of other gases, as shown in Figures 4 and 5. This is also shown in Table 3 in the form of the peculiar values of C_P for all membranes. In the case of Mem.-A, for example, the values of C_P for CO_2, O_2, and N_2 are about 1×10^{-6}, while those of H_2 and He are 1.7×10^{-5} and 7.0×10^{-6}, respectively. Since it can be assumed that C_P in Eq. 19 is related to the geometry of the pores by comparing Eq. 19 with Eq. 7, the difference in C_P probably means the difference in effective pores for permeation. This result can be explained as follows.

In the colloidal sol solutions used in this study, as mentioned in the "Membrane Preparation" section, there exist the first silica colloidal particles, which have network structures that consist of linearly or three-dimensionally grown silica polymers, and the larger particles generated by the secondary growth of the first particles. We therefore might naturally think that the relatively smaller openings were caused by the network structures of the silica polymers (intraparticle pores) and that the larger interparticles pores could be produced on porous ceramic membranes prepared by coating these colloidal sol particles.

Table 3. Values of C_P and E_P in Eq. 19 Obtained from Fittings to Observed Temperature Dependencies of Permeability

		CO_2	O_2	N_2	Ar	CH_4	He	H_2
Mem.-A	E_P [J/mol]	−11,200	−6,200	−5,900	−5,300	−6,300	1,700	−1,300
	$C_P\times10^6$	0.754	1.47	1.09	1.57	0.753	17.19	7.01
Mem.-B	E_P [J/mol]	−9,200	−1,900	10	−100	—	4,000	2,900
	$C_P\times10^6$	0.336	0.834	0.432	0.766	—	22.2	10.9
Mem.-C	E_P [J/mol]	−9,200	−1,500	650	—	—	3,000	2,100
	$C_P\times10^6$	0.761	1.63	1.06	—	—	14.3	9.02
Mem.-C′	E_P [J/mol]	−10,400	−720	2,000	—	—	3,900	2,400
	$C_P\times10^6$	0.173	0.563	0.346	—	—	10.4	4.99

If we suppose that small molecules such as He and H_2 can permeate through both the intra- and interparticle pores, while other larger gas molecules can only permeate through the interparticle pores, the preceding experimental results can be reasonably explained as follows. Since intraparticle openings are very small, and even He and H_2 would feel the repulsive potential from the pore wall, molecules that have larger kinetic energy are best suited for permeation and the permeance increases with increasing temperature (activated diffusion). On the other hand, in larger interparticle pores, He and H_2 molecules, which have little affinity with the pore surface, permeate based on the Knudsen diffusion mechanism, and the permeance decreases with increasing temperature. The relative magnitude of the amount permeated through these two types of pores determines whether the overall temperature dependence is positive or negative. Actually, for Mem.-A, whose mean pore size would be larger than those of the others, a large number of He and H_2 molecules could permeate through interparticle pores and the absolute values of E_P were relatively small compared with those on other membranes. This means that "activation energy" for permeation of these gases is small on Mem.-A. In addition, the permeance of H_2, whose molar weight is smaller than that of He, was larger than He permeance on Mem.-A. This is true for permeation according to the Knudsen mechanism. On the other hand, on Mem.-B, -C, and -C′, whose mean pore size would be smaller than that of Mem.-A, the relative magnitude of permeance of smaller molecules through intraparticle openings could be larger, and the apparent activation energy for permeation of these gases was larger than that on Mem.-A. This might indicate that the activated diffusion mechanism was dominant for permeation of He and H_2 on Mem.-B, -C, and -C′. This assumption also could be supported by the fact that in the high-temperature region, the permeance of He, whose molecular size is smaller than that of H_2, is larger than H_2 permeance on Mem.-B, -C, and -C′.

It should also be noted that the permeances of He and H_2 are much larger than those of other gases on all membranes. Since intraparticle openings have the overwhelming majority of all pores on a membrane, the overall permeance of those gas molecules that manage to permeate through those small openings could be relatively large, in spite of the small permeance of the He and H_2 molecules through one intraparticle opening.

Judging from the preceding results and considerations, the permeation mechanism of CO_2 may be of Type II in Figure 2 for both Mem.-A and Mem.-B, while O_2 and N_2 are Type II on Mem.-A and Type III on Mem.-B. Helium probably permeated predominantly through the smaller pores, or the dense phase (intraparticle space), as Type IV.

Prediction of the permeation ratio of CO_2/N_2 as a function of pore size

Permeance is affected by the interaction between a permeating molecule and a pore surface, which, in Eq. 19, varies with the pore size via E_P. In this section, the dependence of a potential field in a micropore on pore diameter is studied quantitatively by using experimental permeation data, and the effect of the pore size on selectivity for CO_2/N_2 separation is predicted based on the gas-permeation model.

Assuming that the interaction between the diffusant and the pore can be accounted for by the Lennard-Jones potential, the potential is described by Eq. 20

$$E_P/\epsilon_{gs} = 4m\left[\left(\frac{\sigma_{gs}}{r_P}\right)^{12} - \left(\frac{\sigma_{gs}}{r_P}\right)^{6}\right], \tag{20}$$

where r_P is the pore radius (the distance from the center of the pore to the center of an oxygen atom on the pore surface); ϵ_{gs} and σ_{gs} are energy and size parameters, respectively; and m indicates a parameter pertaining to the overlapping of the gas–(silica surface oxygen) interaction potential. The strict potential function within a slit or cylindrical pore can be given analytically (Everet and Powl, 1976; Peterson et al., 1986), and model calculations of molecular transport through small pores were performed by Petropoulos and Petrou (1991) by using that function. However, those analytical functions contain the surface or volume densities of molecules that consist of the bulk membrane as parameters, and the infinite series or integration term appears in an analytical form that which gives the potential field. Therefore it is difficult to handle the model equation from the point of view of engineering or actual application. On the other hand, Xiao and Wei (1992a), and Shelekhin et al. (1995) expressed approximately the activation energy of diffusion within a micropore of zeolite and molecular-sieve glass membrane, respectively, by using a Lennard-Jones-type potential function. In their studies, the pore neck consisted of oxygen atoms-ring and the number of those atoms was given as a constant. Xiao and Wei used the value of eight for the eight-membered ring of zeolite 5A and ten for the ten-membered ring of ZSM-5. Shelekhin et al. also adopted the number of eight oxygen atoms. Since the parameter m in Eq. 20 originally indicated the overlapping effect of the gas–solid interaction potential, we assumed that it should be a variable parameter that depends on pore size. The applicability of the simple approximated form of Eq. 20 was examined as to whether it could express not only activated gas permeation but also a surface-diffusion-like tendency through several porous membranes that had slightly different pore diameters from each other.

Figure 8 shows the relation between the experimentally obtained value of E_P in Table 3 and σ_{gs}. Using potential parameters summarized in Table 4 (Brodka and Zerda, 1991; Shelekhin et al., 1995), the gas–solid potential parameters can be estimated by the following combining rule (Steele, 1974), where a permeating gas molecule is thought of as interacting oxygen atoms on the silica surface:

$$\epsilon_{gs} = \sqrt{\epsilon_g \epsilon_O} \tag{21}$$

$$\sigma_{gs} = \frac{\sigma_g + \sigma_O}{2}. \tag{22}$$

The solid and broken curves in the figure are fitted ones by Eq. 20 for Mem.-A, -B, and -C′, with m and r_P as the fitting parameters. All fitted curves increase abruptly at a specific σ_{gs}, and the σ_{gs} of Mem.-A is larger than that of Mem.-B and -C′. The values of fitted parameters m and r_P for each membrane are shown in Table 5 with the values for Mem.-C.

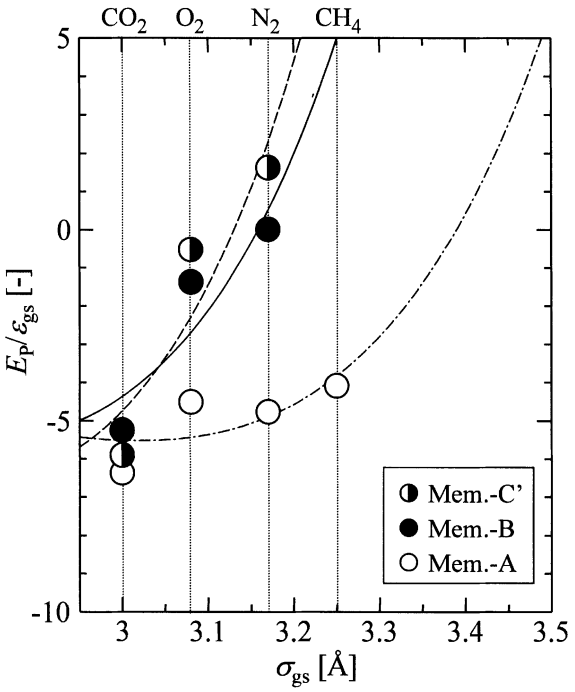

Figure 8. E_P vs. size parameter of Lennard-Jones potential, σ_{gs}.

Table 4. Lennard-Jones Potential Parameters

	CO_2	O_2	N_2	CH_4	O*
ϵ_i/k [K]	195.2	118	95.05	148.2	230
σ_i [Å]	3.3	3.46	3.64	3.8	2.7

Source: Shelekhin et al., 1995.
Note: $i = g, o$.
*Brodka and Zerda, 1991.

Except for the size of surface atoms, the effective mean pore diameter, d_e, is $d_e = 2r_P - \sigma_O = 4.08$, 3.62, 3.60 and 3.56 Å for Mem.-A, -B, -C and -C′, respectively. As expected from Figure 3, Mem.-B appears to have smaller pores than Mem.-A. This slight difference in mean pore diameter (about 0.5 Å) might cause an appreciable difference in permeation characteristics of Ar, O_2, and N_2 between Mem.-A and Mem.-B.

There is another point to be noted in Table 5. The value of m increases with a decrease in r_P. The relations between m and r_P are plotted in Figure 9. This is very reasonable, since the parameter m is not necessarily equal to the number of oxygen atoms, which consist of the pore circumference, indicating the overlapping effect of the potential by close pore

Table 5. Fitted Parameters in Eq. 20 for the Cases of Mem.-A, -B, -C, and -C′

	m [−]	r_P [Å]	d_e ($= 2r_P - \sigma_o$) [Å]
Mem.-A	5.52	3.39	4.08
Mem.-B	5.60	3.16	3.62
Mem.-C	5.74	3.15	3.60
Mem.-C′	6.78	3.13	3.56

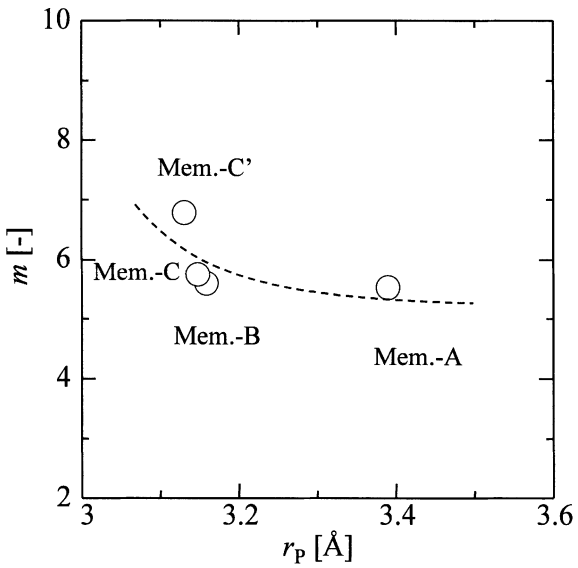

Figure 9. Dependence of pair-potential overlapping effect on pore size.

walls. If the pore diameter is sufficiently small, the potential from the inner oxygen atoms of the pore wall should be significant.

Figure 10 shows the E_P vs. r_P curves for CO_2 and N_2 calculated from Eq. 20 by using m fitted as described earlier. The value of d_e, which corresponds to r_P, is indicated on the upper axis. We note that the depth of the potential well for the CO_2 curve is deeper than that for N_2, and that r_P, which gives a potential minimum, is smaller for CO_2. This means

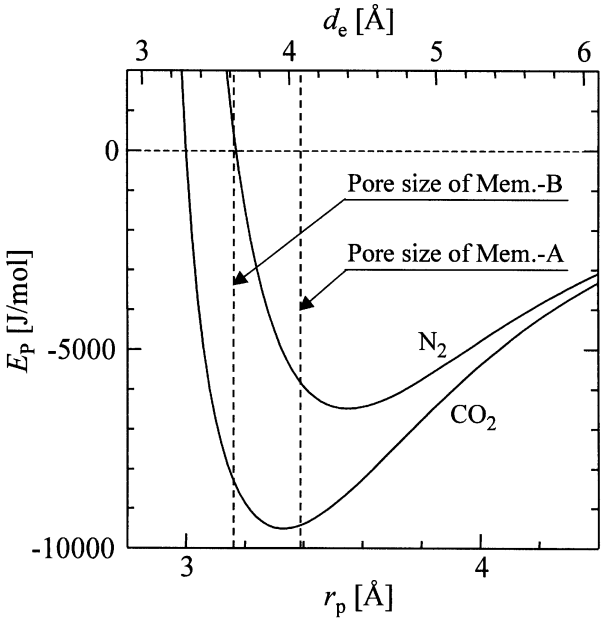

Figure 10. Depth of leveled mean potential of CO_2 and N_2 in micropore as a function of pore size calculated from Eq. 20.

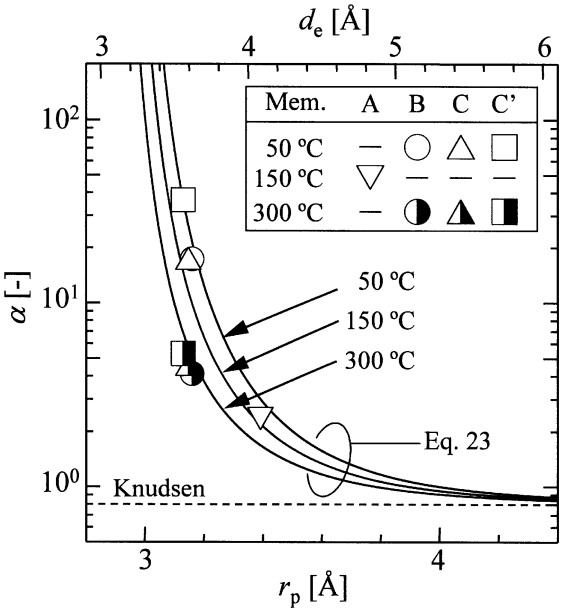

Figure 11. Dependencies of CO_2/N_2 permeation ratio on pore size and temperature predicted by Eq. 23 (curves predicted by Eq. 23; points experimental).

not only that CO_2 interacts more strongly with the silica surface than N_2, but also that CO_2 is susceptible to attractive potential, even in smaller pores, whereas N_2 is subject to only a slight attractive or even repulsive potential. The broken lines in the figure indicate the r_P of Mem.-A and Mem.-B shown in Table 5. At r_P of Mem.-A, the difference between E_P of CO_2 and that of N_2 is not so strikingly large. As for Mem.-B, the potential for CO_2 is still attractive, while nearly no effective interaction exists for N_2. The result of this calculation is consistent with the experimental permeation data for Mem.-A and Mem.-B.

Based on the gas-permeation model mentioned earlier, we calculated the permeation ratio α of CO_2/N_2 from the potential curves in Figure 10. Assuming that CO_2 and N_2 permeate the same pores, and that C_P in Eq. 19 is identical, α can be given by Eq. 23:

$$\alpha = \frac{P_P^{CO_2}}{P_P^{N_2}} = \left(\frac{M_{N_2}}{M_{CO_2}}\right)^{0.5} \exp\left(-\frac{E_P^{CO_2} - E_P^{N_2}}{RT}\right). \quad (23)$$

The dependence of α on r_P and temperature calculated from Eq. 23 are shown in Figure 11. Permeation ratio α becomes smaller with increasing temperature; it is only 2 or 3 even for Mem.-B at 300°C. It is also sensitive to pore diameter, and is rather large for pores smaller than 4 Å in effective pore diameter d_e, while, for pores larger than 5 Å, an increase of α cannot be expected and, according to the model, gradually approaches the value of the Knudsen mechanism. In such large pores, however, the homogeneous potential model introduced here would fail, since in pores where two or more molecules can be arranged in a radial direction, the potential minimum does not exist at the center of the pore, but is instead near the pore wall. In such large pores, we can expect a permeance that is a little larger than that by the Knudsen mechanism; however, the enhancement may not be so striking as in much smaller pores where the depth of the potential well is a great deal deeper. Judging from the curves in Figure 11, for this type of sol–gel-derived silica membrane, it may be difficult to obtain a value of α of over 100 at high temperature, while at relatively low temperature, it might be possible to obtain several tens of α by preparing such a membrane with pores of around 3.6 Å, as is the case for Mem.-B. In addition, if the energy difference of $E_P^{CO_2} - E_P^{N_2}$ can be larger, by using some material that has more affinity with CO_2, for example, an improvement in selectivity can be expected, according to Eq. 23.

Conclusion

Sol–gel-derived microporous silica membranes prepared in this study showed high performance in CO_2 gas permeance and a permeation ratio of CO_2/N_2. For example, on Membrane C′, the value of CO_2 permeance was 7.0×10^{-7} mol/m^2·s·Pa, and the permeation ratio of CO_2/N_2 was 36 at 50°C. Gas permeation properties on those membranes were analyzed by using a simple gas-permeation model to consider the effect within a micropore of the attractive and repulsive potential field on permeating gas molecules and the Knudsen diffusivility of those molecules. The permeation properties of several gases are consistent with the model. In addition, by assuming the Lennard-Jones-type potential between a permeant molecule and a silica surface, the effective pore diameters of membranes were evaluated and the potential curves of CO_2 and N_2 within a silica pore were calculated as a function of pore size. From this model calculation, the permeation ratio of CO_2/N_2, α, was evaluated and the effect of the pore size, and the interaction between a molecule and pore surface on α was quantitatively studied. This reinforced the importance of these factors on CO_2/N_2 gas separation. In order to improve the permeation ratio of CO_2/N_2, the precise pore-size control and the development of membrane materials that have a greater interaction with CO_2 may be required.

Notation

$a(x)$ = acceleration as a function of location x, m/s^2
A = gas-phase flow coefficient, defined by Eq. 1
B = surface flow coefficient, defined by Eq. 1
c = gas concentration, mol/m^3
C = geometrical factor
C_A = frequency factor for activated diffusion, defined by Eq. 9, mol/m^2·s·Pa
C_K = geometrical coefficient, defined by Eq. 8
C_P = geometrical coefficient, defined by Eq. 19
d = pore diameter, m
d_e = effective pore diameter, m
D = Fickian diffusivity, m^2/s
E = apparent activation energy, J/mol
E_A = activation energy, J/mol
E_P = potential in the pore, J/mol
J = diffusive flux, mol/m^2·s
L = distance across the membrane, m
m = overlapping parameter for the gas–(silica surface oxgen) interaction potential

M = molecular weight, kg/mol
Δp = pressure difference, Pa
Δp_a = apparent pressure drop across the membrane, Pa
Δp_P = effective pressure drop in the pore, Pa
p = pressure, Pa
p_0 = bulk phase gas pressure, Pa
p_P = pressure in the pore, Pa
P_A = apparent activated permeability (permeance) coefficient, mol/m^2·s·Pa
P_{obs} = experimentally observed permeability (permeance) coefficient, mol/m^2·s·Pa
P_K = Knudsen permeability (permeance) coefficient, mol/m^2·s·Pa
P_P = permeability (permeance) coefficient, defined by Eq. 19, mol/m^2·s·Pa
r_P = pore radius, m
R = gas constant, J/mol·K
T = absolute temperature, K
$\bar{v}$ = mean molecular velocity, m/s

Greek letters

Δ = difference between adsorption energy and activation energy, J/mol
ϵ = Lennard-Jones potential energy parameter, J
λ = mean free path, m
$\rho(x)$ = gas density as a function of location x, mol/m^3
σ = Lennard-Jones potential size parameter, m
Ψ = external potential, J

Superscripts and subscripts

g = gas molecule
o = oxygen atom on silica surface
gs = gas–(silica surface) interaction
u = upstream
d = downstream

Literature Cited

Asaeda, M., K. Okazaki, and A. Nakatani; "Preparation of Thin Porous Silica Membranes for Separation of Non-Aqueous Organic Solvent Mixtures by Pervaporation," *Ceram. Trans. Porous Mater.*, **31**, 411 (1993).

Breck, D. W., *Zeolite Molecular Sieves*, Wiley, New York (1974).

Brodka, A., and T. W. Zerda, "Molecular Dynamics of SF_6 in Porous Silica," *J. Chem. Phys.*, **95**, 3710 (1991).

Brunauer, S., P. H. Emmett, and E. Teller, "Adsorption of Gases in Multimolecular Layers," *Amer. Chem. Soc.*, **60**, 309 (1938).

Burggraaf, A. J., "Single Gas Permeation of Thin Zeolite (MFI) Membranes: Theory and Analysis of Experimental Observations," *J. Membr. Sci.*, **155**, 45 (1999).

Everett, D. H., and J. C. Powl, "Adsorption in Slit-Like and Cylindrical Micropores in the Henry's Law Region," *J. Chem. Soc. Faraday Trans. I*, **72**, 619 (1976).

Hwang, S. T., and K. Kammermeyer, "Surface Diffusion in Microporous Media," *Can. J. Chem. Eng.*, **44**, 82 (1966).

Lange, R. S. A., K. Keizer, and A. J. Burggraaf, "Analysis and Theory of Gas Transport in Microporous Sol-Gel Derived Ceramic Membranes," *J. Membr. Sci.*, **104**, 81 (1995).

Li, D., and S. T. Hwang, "Preparation and Characterization of Silicon Based Membrane for Gas Separation," *J. Membr. Sci.*, **59**, 331 (1991).

Li, D., and S. T. Hwang, "Gas Separation by Silicon Based Inorganic Membrane at High Temperature," *J. Membr. Sci.*, **66**, 119 (1992).

Nicholson, D., and J. H. Petropoulos, "Influence of Adsorption Forces on the Flow of Dilute Gases Through Porous Media," *J. Colloid Interface Sci.*, **45**, 459 (1973).

Petropoulos, J. H., and V. I. Havredaki "On the Fundamental Concepts Underlying Henry-Law Adsorption and Adsorbed Gas Transport in Porous Solids," *J. Chem. Soc., Faraday Trans. 1*, **82**, 2531 (1986).

Petropoulos, J. H., and J. K. Petrou, "Simulation of Molecular Transport in Pores and Pore Networks," *J. Chem. Soc. Faraday Trans.*, **87**, 2017 (1991).

Peterson, B. K., J. P. R. B. Walton, and K. E. Gubbins, "Fluid Behaviour in Narrow Pores," *J. Chem. Soc., Faraday Trans. 2*, **82**, 1789 (1986).

Shelekhin, A. B., A. G. Dixon, and Y. H. Ma, "Theory of Gas Diffusion and Permeation in Inorganic Molecular-Sieve Membranes," *AIChE J.*, **41**, 58 (1995).

Shindo, Y., T. Hakuta, H. Yoshitome, and H. Inoue, "Gas Diffusion in Microporous Media in Knudsen's Regime," *J. Chem. Eng. Jpn.*, **16**, 121 (1983).

Steele, W. A., *The Interaction of Gases with Solid Surfaces*, Pergamon Press, Oxford (1974).

Xiao, J., and J. Wei, "Diffusion Mechanism of Hydrocarbons in Zeolites: I. Theory," *Chem. Eng. Sci.*, **47**, 1123 (1992a).

Xiao, J., and J. Wei, "Diffusion Mechanism of Hydrocarbons in Zeolites: II. Analysis of Experimental Observations," *Chem. Eng. Sci.*, **47**, 1143 (1992b).

Yoshioka, T., E. Nakanishi, T. Tsuru, and M. Asaeda, "Permeation Mechanism of Inorganic Gases in Ultra-Microporous Silica Membranes, *Proc. Int. Conf. Inorganic Memb. ICIM-5*, Nagoya, Japan, p. 120 (1998).

Manuscript received June 5, 2000, and revision received Mar. 26, 2001.